Electronic supplementary information for:

Electrochemically Reversible Lattice with Redox Active A-site of Double Perovskite Oxide Nanosheets to Reinforce Oxygen Electrocatalysis

*Rahul Majee,[#] Quazi Arif Islam,[#] Surajit Mondal and Sayan Bhattacharyya**

Department of Chemical Sciences, and Centre for Advanced Functional Materials, Indian Institute of Science Education and Research (IISER) Kolkata, Mohanpur - 741246, India

#Equal contribution
*Email for correspondence: sayanb@iiserkol.ac.in

Experimental Section

Materials

Praseodymium acetate [$Pr(NO_3)_3$, Alfa Aesar, 99%], barium nitrate [$Ba(NO_3)_2$, Alfa Aesar, 99%], cobalt nitrate hexahydrate [$Co(NO_3)_2.6H_2O$, Merck, 99%], manganese acetate tetrahydrate [$Mn(CH_3COO)_2.6H_2O$, Merck, 99%], glycine (Merck, 99%) were used without further purification. Distilled water was used during synthesis and electrochemical tests unless specified. Potassium hydroxide (KOH, Merck, 98%) was used to prepare the electrolyte.

Synthesis of $BaPrMn_2O_{5+\delta}$ (BPM)

For the synthesis of BPM, nitrate salts of Ba, Pr and Mn-acetate in 1:1:2 mole ratio were dissolved and mixed in distilled water. pH of the clear solution was adjusted to 6.5 by adding dilute ammonia followed by which glycine was added under stirring. The molar ratio of metal precursors and glycine was kept at 1:1 while for modulation the ratio was varied as 1:0.5 and 1:1.5, keeping the pH 6.5. The solution was then heated at 80°C to evaporate the solvent forming the BPM gel. The gel was further heated to obtain a gray powder which was dried at 150°C for 2 h. The dried powder was calcined at 950°C for 5 h in air followed by reduction at 750°C for 5 h in 5% H_2 in Ar mixture gas to obtain the pure phase of BPM.

Synthesis of $BaPrCo_2O_{5+\delta}$ (BPC)

BPC was synthesized using a similar procedure as above with the only exception of using 2 mmol of $Co(NO_3)_2.6H_2O$instead of $Mn(CH_3COO)_2.6H_2O$.

Synthesis of $BaPrMn_{2-x}Co_xO_{5+\delta}$ (BPCM)

Using a similar procedure as that of BPM and BPC, different compositions of BPCM (viz. x = 0.25, 1 and 1.75) were obtained by varying the Co:Mn ratio but keeping the Ba and Pr concentrations constant. Therein the obtained catalysts are $BaPrMn_{1.75}Co_{0.25}O_{5+\delta}$ (BPMC-0.25), $BaPrMnCoO_{5+\delta}$ (BPMC-1) and $BaPrMn_{0.25}Co_{1.75}O_{5+\delta}$ (BPMC-1.75).

Thermal oxidation of BPMC-0.25

To circumvent the oxygen deficiency, BPMC-0.25 was annealed at 500°C in presence of O_2 (10 sccm) flow for 1h to produce BPMC-0.25-Ox.

Physicochemical characterization

Powder X-ray diffraction (PXRD) patterns were recorded with Rigaku Smart Lab (mini flex II) X-ray diffractometer. Cu Kα (λ=1.5403 Å) target was used for diffraction with Bragg Brentano

filter and Dtex 1D detector. Scan rate was maintained at 2θ = 5°/min for all measurements except for the data used for Rietveld refinements wherein data acquisition was done at scan rate 2θ = 1°/min. Rietveld refinements were performed using GSAS-II software and fitting was finalized when best possible minimum weighted residual (R_{wp}) was achieved. Three dimensional visualization of corresponding crystal structures were obtained from Vesta software using the refined *cif* files. Transmission electron microscopy (TEM) analyses were performed in JEOL 2100F electron microscope (IISER Kolkata DST-FIST facility) at an operating acceleration voltage 200 kV and corresponding elemental maps were obtained using Oxford X-max solid state Si drift X-ray detector. For preparing the TEM samples, the powder was dispersed in isopropanol without any sonication followed by drop casting the supernatant solution on carbon coated Cu grid (Ted Pella, 300mesh). To check surface topology and NS thickness, the samples were mildly sonicated in isopropanol then drop casted on clean Si substrate. Thereafter atomic force microscopy (AFM) was performed using Nova NT-MDT instrument. Post processing of the AFM data was done using the interfaced software. FESEM images were recorded with Carl Zeiss SUPRA 55VP FESEM instrument. Fourier transform infrared (FTIR) spectral measurements were performed using PerkinElmer spectrum RX1 with KBr pellets. XPS studies were performed using a commercial photoelectron spectrometer PHI 5000 Versa ProbeII, FEI Inc, IIT Kanpur using Al Kα (1486.6 eV) excitation source.

Oxygen non-stoichiometry (δ) determination

Oxygen non-stoichiometry was measured by iodometric titration. Briefly, 100 mg of perovskite oxide sample was dissolved in conc. HCl under Ar atmosphere. Followed by the addition of excess KI (SRL, 98%), KI gets oxidized to I_2 which is equivalent to the number of B-site cations with higher oxidation state getting reduced by accepting one electron. The evolved I_2 was titrated immediately using prior standardized thiosulphate solution. The mole of thiosulphate consumed is equivalent to the mole of B^{3+} cations, which leads to the calculation of δ.[S1,S2]

Oxygen electrocatalysis

In order to examine the electrocatalytic OER and ORR activity of BPMC samples and $Ba_{0.6}Sr_{0.4}Co_{0.8}Fe_{0.2}O_{3-\delta}$ (BSCF),[S3] catalyst inks were prepared by dispersing BPMC/BSCF with nafion as binder and aqueous isopropanol as solvent. A measured amount of catalyst ink (0.5 mg/cm^2) was drop-casted onto the carbon cloth of area 0.3 cm^2 to check OER, and on RRDE

with 5mm diameter for measuring ORR activity. The electrolyte was KOH (1M for OER and 0.1 M for ORR) while Ag/AgCl (3 M KCl) and platinum wire was used as reference and auxiliary electrode, respectively. Linear sweep voltammograms (LSVs) were collected at 10 mV/s potential sweep rate. The uncompensated solution resistance was measured at 85% compensation level and the applied potential was corrected accordingly.[S3] The stability of the Ag/AgCl (3 M KCl) reference electrode during measurement conditions was affirmed from cyclic voltammograms (CV) with standard potassium ferricynide solution before and after at least 100 CV cycles (see Figure S21). The Tafel plots were obtained from the LSV plots. Electrochemical impedance spectroscopy (EIS) measurements were performed at bias voltage of 1.6 and 0.5 V with respect to reversible hydrogen electrode (RHE) for OER and ORR, respectively. Chronopotentiometric stability test was performed after loading the catalyst ink on CFP; with 10 and -1 mA/cm^2 constant current density being considered for OER and ORR, respectively. Double layer charge capacitance (C_{dl}) values were obtained after executing the CV cycles at non faradic region with variable scan rates and equation (S1) was used for the calculation of C_{dl}.

$C_{dl} = (I \times t)/V = I/v$ F (S1)

Reversible O-content estimation

The reversibility of oxygen content in BPMC-0.25 was carried out through electrochemical oxidation and reduction CV cycles in oxygen saturated 0.1M KCl. BPMC-0.25 loaded on Ni-foil substrate was subjected to oxidative and reductive cycles in the potential window 0 to 0.8 and 0 to -0.8 V versus normal hydrogen electrode (NHE), respectively. Oxidized samples were collected after 20, 50 and 100 cycles to obtain BPMC-ox20, BPMC-ox50 and BPMC-ox100, respectively. Concurrently reduced samples were obtained by oxidation followed by equal number of reduction cycles, e.g. successive *n* oxidative and *n* reductive cycles (*n* = 20, 50 and 100) gave three reduced samples viz. BPMC-ox20/red20, BPMC-ox50/red50 and BPMC-ox100/red100. The next round of successive oxidation produces BPMC-ox20(2), BPMC-ox50(2) and BPMC-ox100(2) samples, respectively. At each step PXRD was used to investigate the change in phase and crystal structures. The impact of such *exsitu* oxidation and reduction of BPMC-0.25 on oxygen electrolysis was examined in 0.1M KOH electrolyte and the structural changes were elucidated again by PXRD.

To compare the impact of *insitu* oxidation and reduction on oxygen electrolysis in 0.1M KOH electrolyte, 50 CV cycles between 1.2 to 1.8 V at 100 mV/s scan rate were performed prior

to executing ORR and successive OER. Concurrently 50 CV cycles between 1 to 0.2 V at the same scan rate were performed before measuring OER and successive ORR. PXRD patterns were collected at each step of the experiments. The comparison the O_2 electrocatalytic activity of BPMC-0.25, BPMC-0.25-ox and BPMC-0.25-solid state samples was performed following the above procedure.

Rechargeable Zn-air battery fabrication and testing:

A homemade Zn-air battery set up was employed with a polished Zn plate (thickness = 0.25mm) as the anode and BPMC-0.25 catalyst ink coated carbon cloth (1 mg/cm^2) as the cathode. The electrolyte used was 0.2M zinc acetate solution in 6M KOH. Polarization plots were obtained by performing LSV with 5 mV/s scan rate.

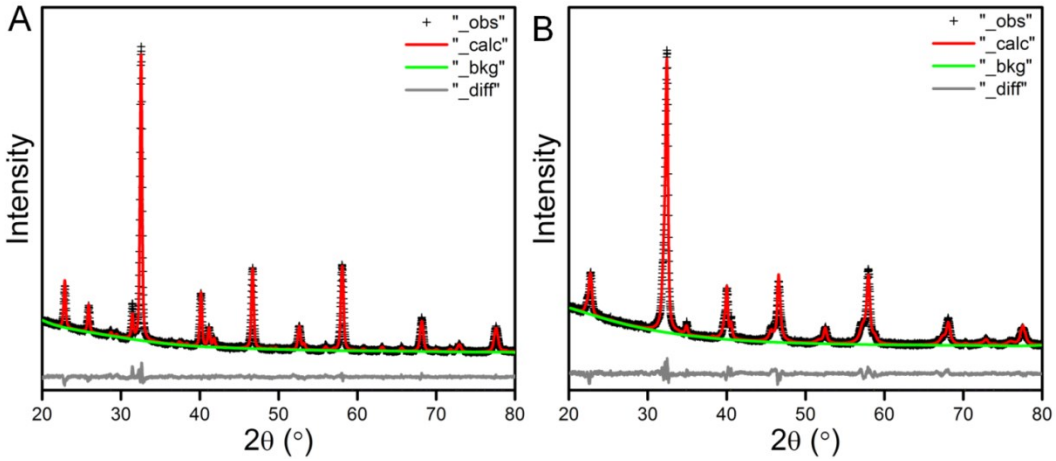

Figure S1. Rietveld refinement of PXRD patterns of (A) BPM-cal and (B) BPM double perovskite.

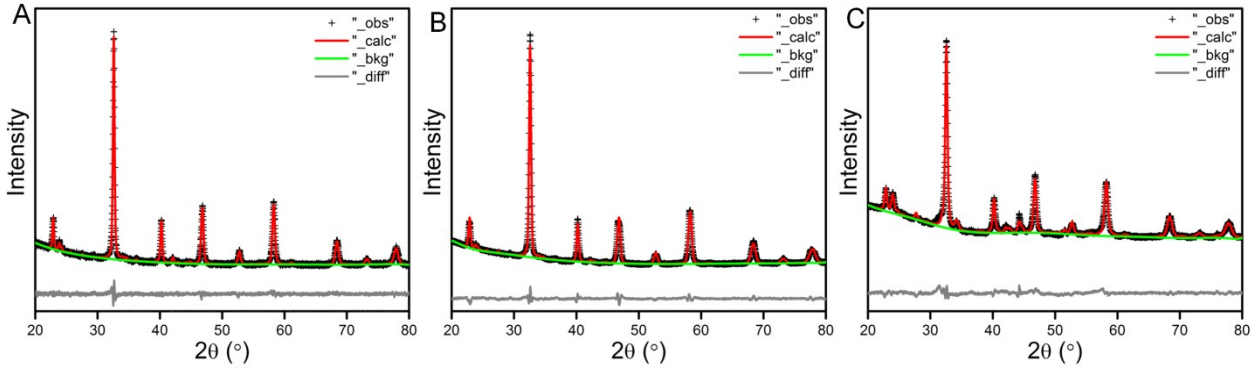

Figure S2. Rietveld refinement of PXRD patterns of Co doped BPM: (A) BPMC-0.25, (B) BPMC-1 and (C) BPM-1.75.

Table S1. Rietveld refinement results.

Sample	Major Phases	Space group	Volume (Å^3)	Lattice parameter (Å)			δ	GOF	R_w
				a	*b*	*c*			
BPM-cal	$BaMnO_3$	*P63/mmc*	135.28	5.6962	5.6962	4.8143	-	1.65	3.05
	$Pr_{0.7}Ba_{0.3}MnO_{3-\delta}$	*Pnma*	236.36	5.5029	7.7953	5.5100	-		
BPM	$BaPrMn_2O_{5+\delta}$ (with 8.3wt% MnO)	*P4/mmm*	119.76	3.8851	-	7.9343	0.4	2.01	3.62
BPMC-0.25	$BaPrMn_{1.75}Co_{0.25}O_{5+\delta}$ (with 6.6wt% $BaCO_3$)	*P4/mmm*	116.52	3.8719	-	7.7723	0.09	1.23	3.01
BPMC-1	$BaPrMn_{1.75}Co_{0.25}O_{5+\delta}$ (with 3.6wt% $BaCO_3$, 1.8wt% $BaMnO_3$, 1.2wt% CoO)	*P4/mmm*	116.9	3.8734	-	7.7920	0.1	4.05	2.79
BPMC-1.75	$BaPrMn_{0.25}Co_{1.75}O_{5+\delta}$ (with12.6wt% $BaCO_3$,6.3wt% $BaMnO_3$, 6wt% Co)	*P4/mmm*	116.6	3.8740	-	7.7703	0.1	4.99	3.05

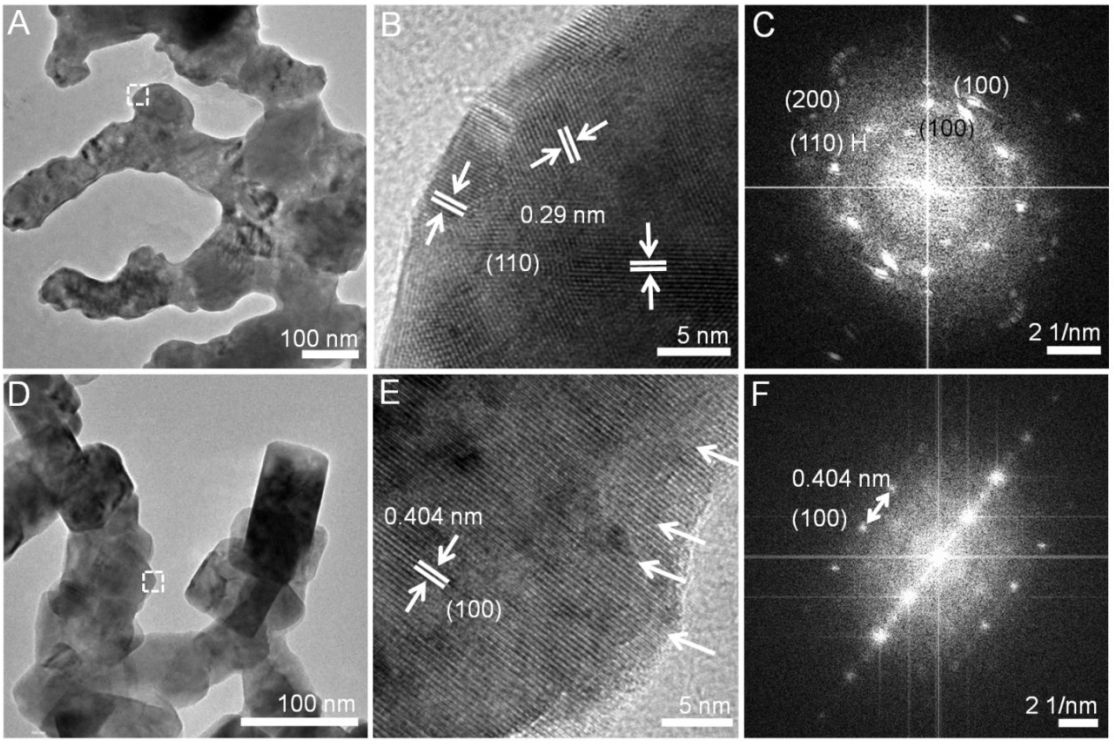

Figure S3. TEM image, HRTEM image and FFT pattern of BPM samples, (A-C) before reduction (BPM-cal) and (D-F) after reduction (BPM NS). The dotted box in (D) shows the region in (E).

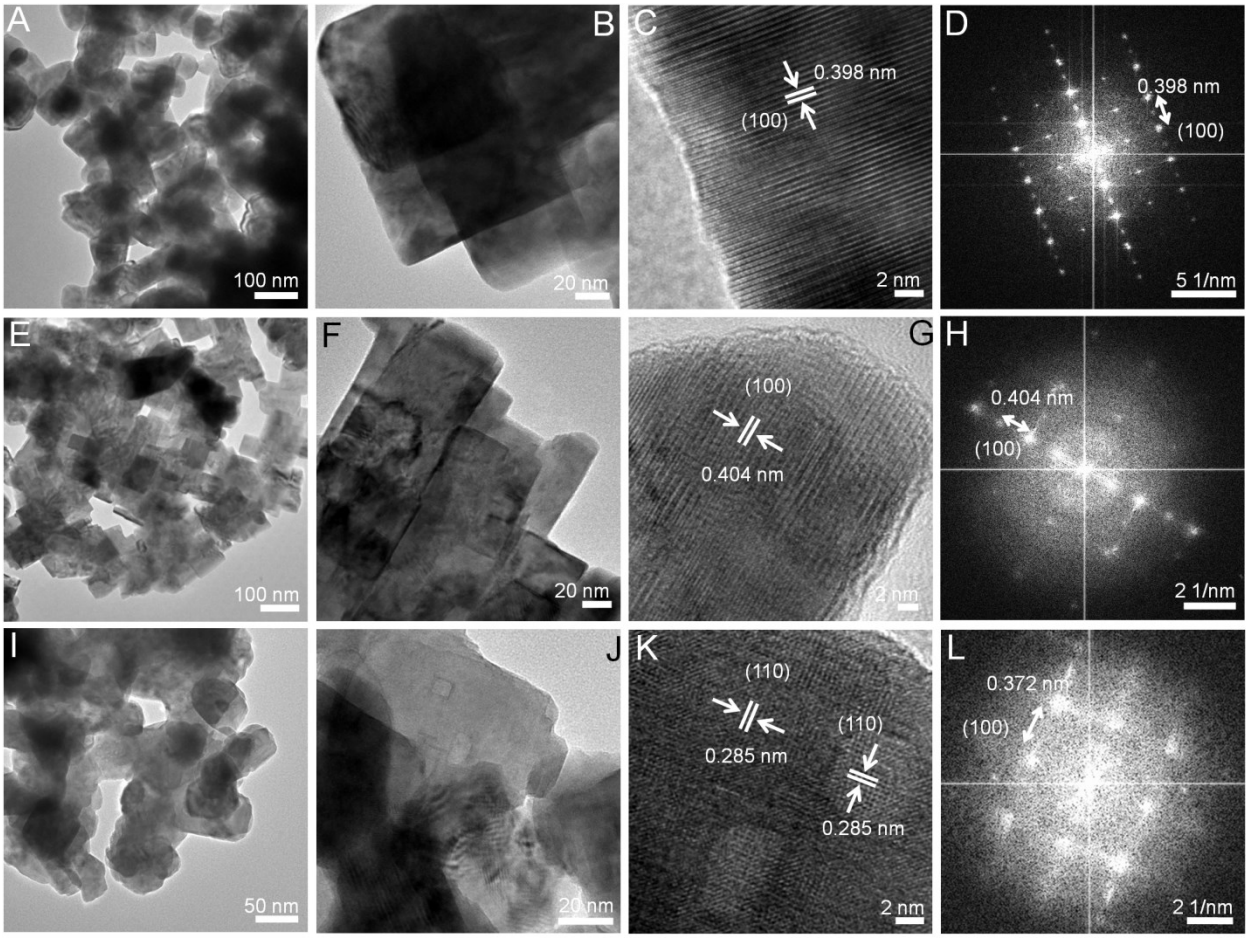

Figure S4. Low, medium and high resolution TEM images along with FFT pattern of Co-doped BPM samples, (A-D) BPMC-0.25, (E-H) BPMC-1 and (I-L) BPMC-1.75.

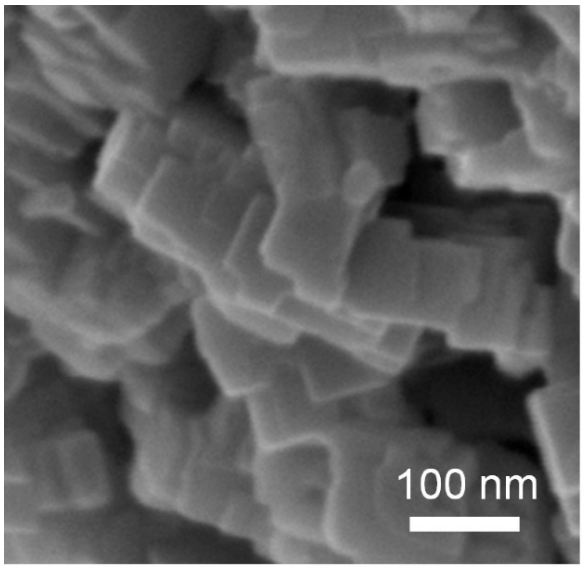

Figure S5. Field emission scanning electron microscope (FESEM) image of BPMC-0.25 NSs.

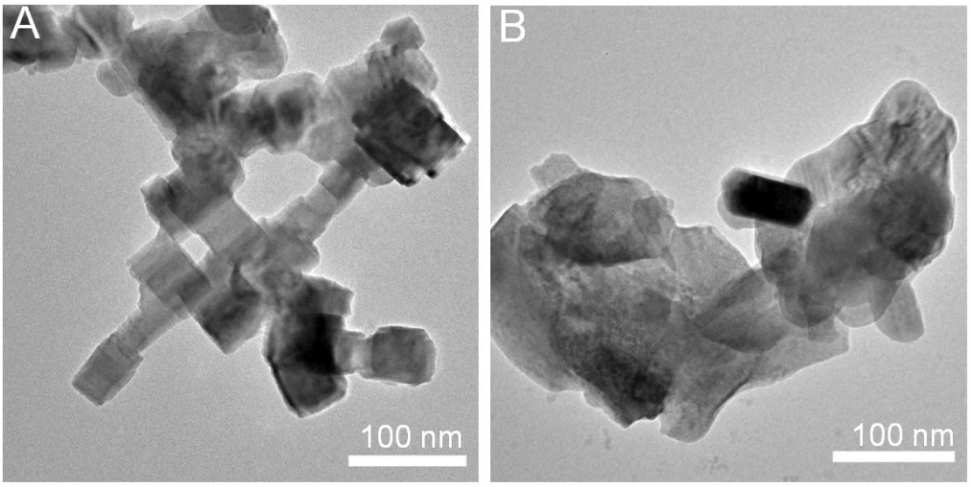

Figure S6. TEM images of (A) BPMC-0.25/1.5×Glycine and (B) BPC.

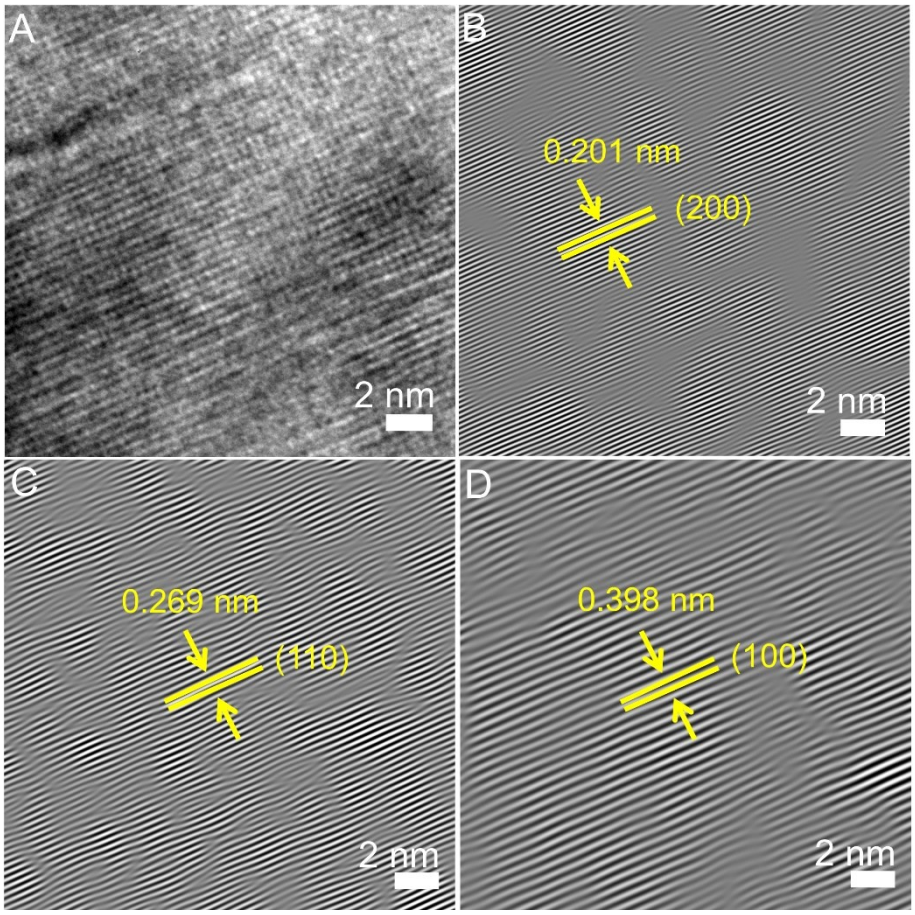

Figure S7. (A) HRTEM image of BPMC-0.25 (repeated from Figure 2B), and its deconvoluted images obtained by using FFT mask filter showing different lattice fringes corresponding to (B) (200), (C) (110) and (D) (100) planes.

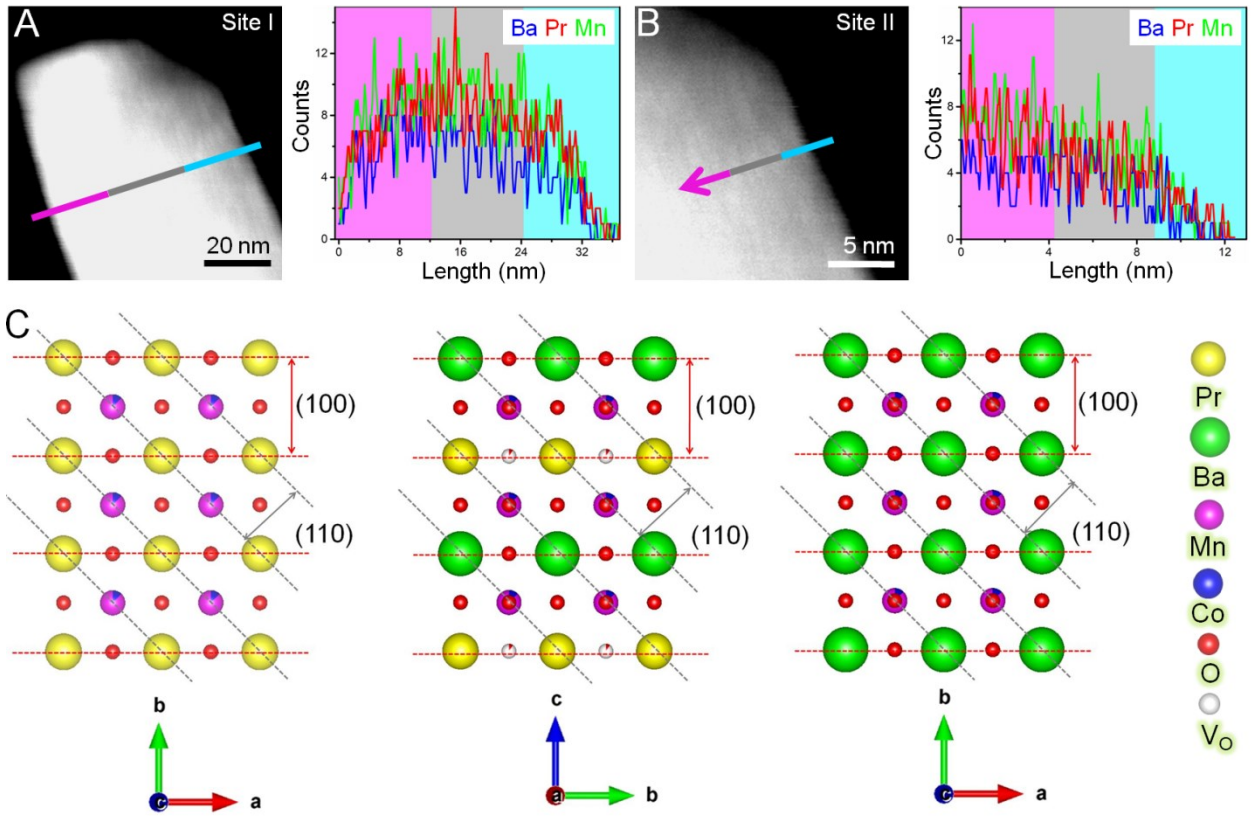

Figure S8. HAADF-STEM images of two different NSs and corresponding line scans (A) through the entire NS and (B) at the surface region. (C) Possibilities of NS termination by Pr in *ab* plane (left), Ba in *ac* or *bc* plane (middle) and Ba in *ab* plane (right). The schematics are drawn considering the abundance of (100) than (110) reflection.

The NS surface exhibits more Pr and Mn counts than Ba. The surface is also abundant with (100) reflection suggesting the PrO_x termination. From the line scan results, Figure S6c (left) shows the most probable structure where the surface is terminated by *ab* plane, with the least abundance of Ba. If the NS surface consists of *ac* or *bc* plane, as in Figure S6c (middle), there will be equal abundance of Ba and Pr, which contradicts the findings in Figure S6a,b. Similarly the possibility of Ba terminated *ab* plane is also not valid as shown in Figure S6c (right).

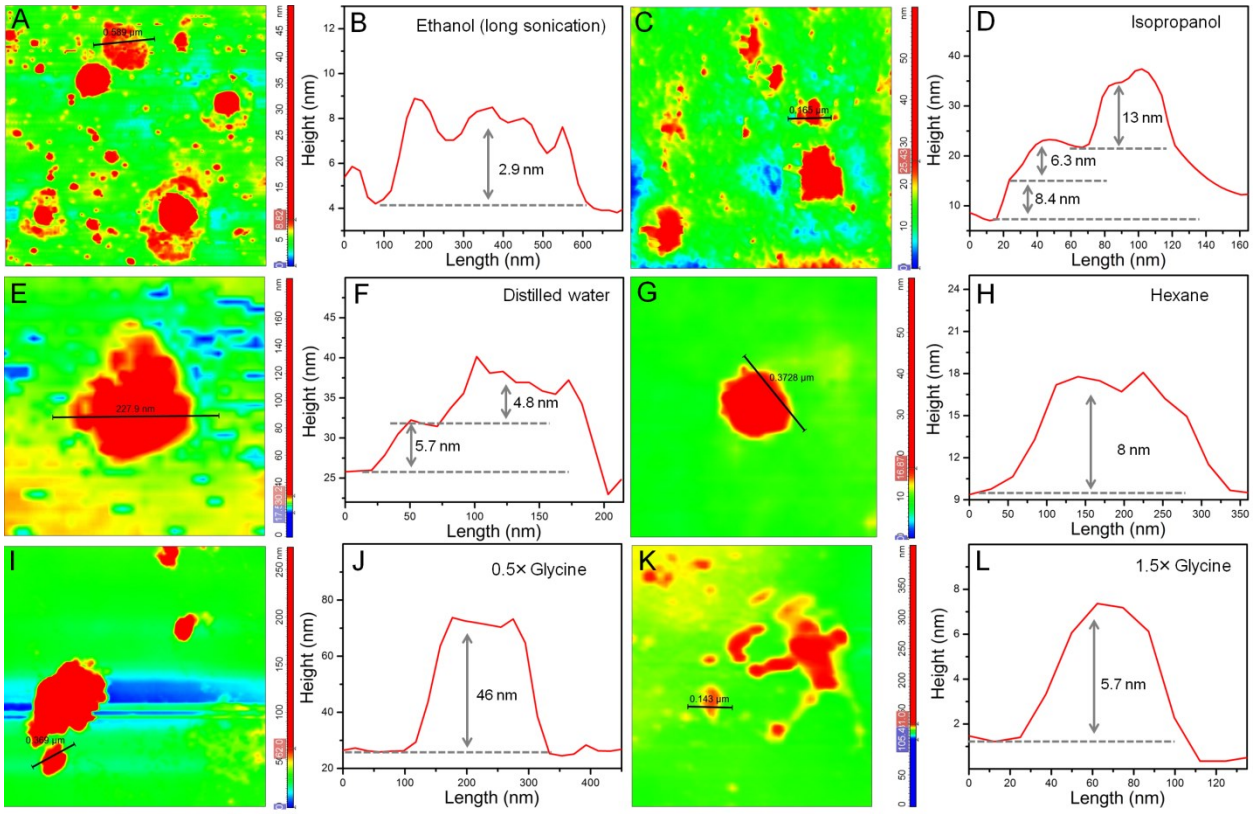

Figure S9. AFM analysis and corresponding height profile of BPMC-0.25 NSs with different dispersing solvents:(A & B)ethanol after long sonication (10 min), (C & D) isopropanol, (E & F) distilled water, (G & H) hexane; and BPMC-0.25 NSs prepared with (I & J) 0.5 times glycine, (K & L) 1.5 times glycine as precursor. In (C-L), the sonication time is 1-2 min.

Table S2. EDS analysis of BPM, BPMC and BPC samples obtained from scanning electron microscope.

Sample	Element (at%)				
	Ba	Pr	Mn	Co	O
BPM	11.2±0.5	11.6±0.8	23.4±1.3	-	53.6±2.6
BPMC-0.25	10.5±0.9	12.2±0.7	14.9±1.4	2.1±0.2	58.8±3.3
BPMC-1	10.4±0.5	11.8±0.5	9.2±0.4	8.4±0.8	60.2±5.2
BPMC-1.75	12.0±0.7	11.5±0.8	1.2±0.3	15.2±0.6	60.1±7.2
BPC	9.2±0.8	10.3±0.6	-	19.3±0.9	61.7±1.3

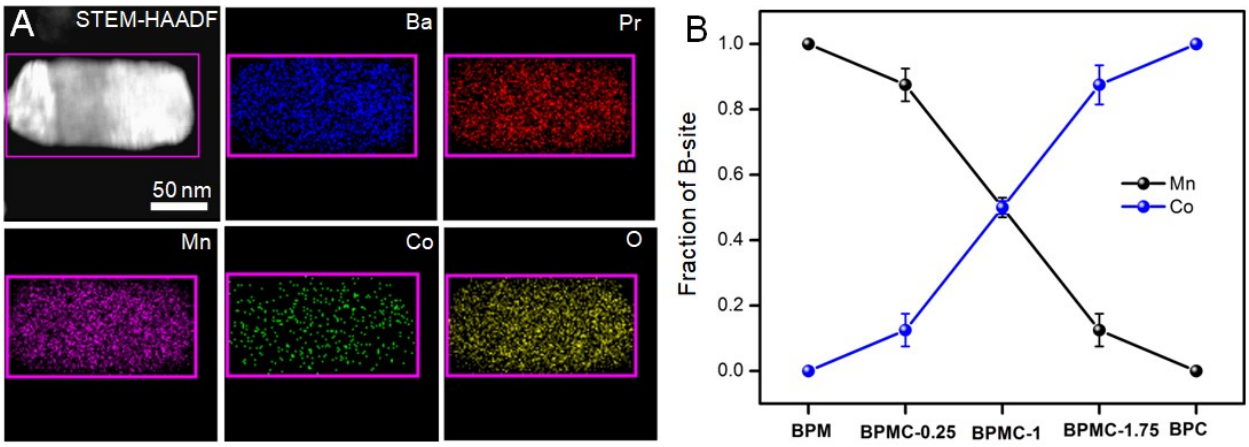

Figure S10. (A) HAADF-STEM EDS elemental mapping on single BPMC-0.25 NS. (B) Fraction of Mn and Co at B-site of BPM, BPMC and BPC samples determined from EDS.

Discussion S1. Iodometric estimation of oxygen non-stoichiometry (δ).

The δ values of $BaPrMn_{1-x}Co_xO_{5+\delta}$ (BPMC) samples were estimated concomitant with previous report:[S1,S2]
Molecular weight of BPMC = M_1 g,
Fraction of B-site ions = $M_{B\ site}/M_1$ g,
Concentration of B-site ions in the sample solution for titration = [B] molar,
Concentration of B^{3+} ion in the sample = $[B^{3+}]$ molar, (determined from iodometry)
Fraction of B^{3+} ion in the sample = $f_{B3+} = [B^{3+}]/[B]$,
Therefore, effective oxidation state of single B-site = $(3 \times f_{B3+}) + [2 \times (1 - f_{B3+})]$
After considering the overall charge neutrality, δ is estimated.

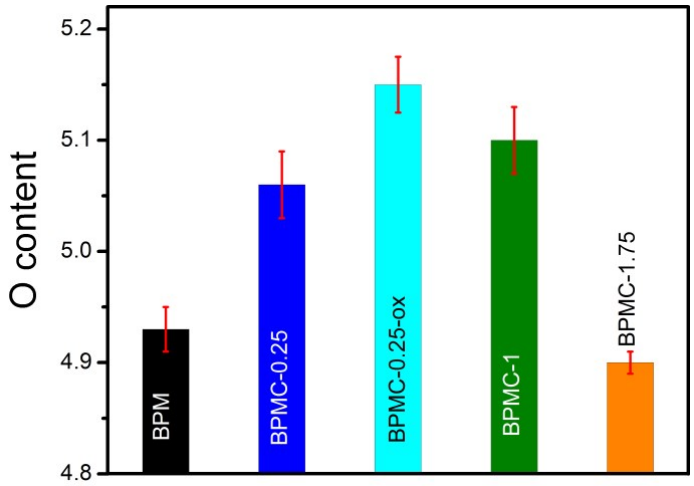

Figure S11. Oxygen nonstoichiometry (δ) calculated from iodometric titration.

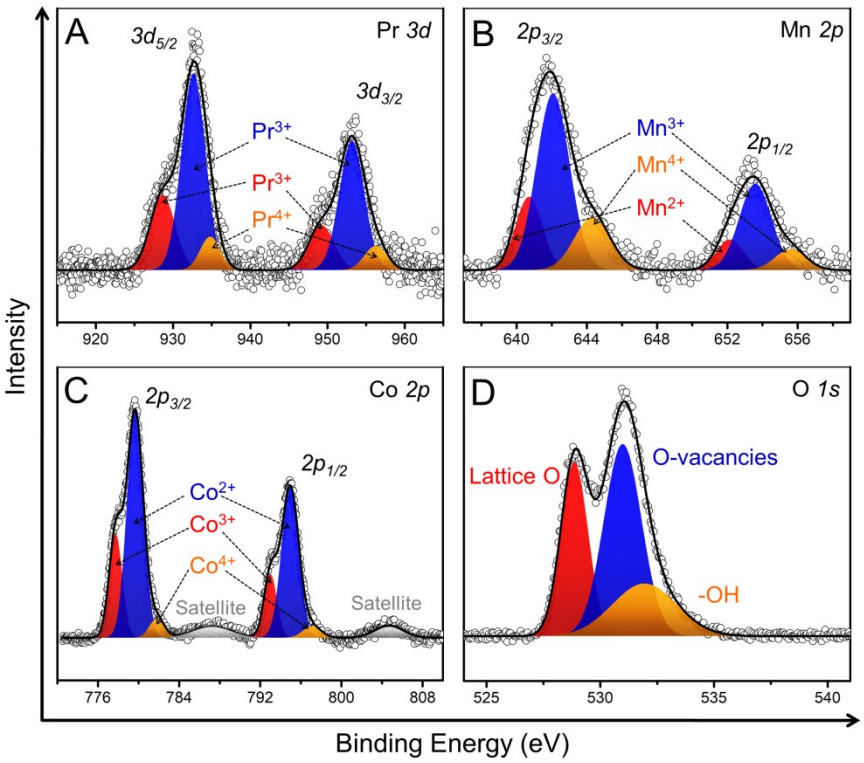

Figure S12. Fitted XPS of BPMC-0.25 NSs: (A) Pr *3d*, (B) Mn *2p*, (C) Co *2p* and (D) O *1s*.

Table S3. XPS fitting parameters of BPMC-0.25 NSs.

Element	State	BE	FWHM	Area
Pr $3d_{5/2}$	Pr^{3+}	928.7	3.83	875.78
		932.6	3.66	2194.77
	Pr^{4+}	934.8	3.06	311.26
Pr $3d_{3/2}$	Pr^{3+}	949.3	3.87	530.19
		953.2	3.81	1501.6
	Pr^{4+}	956.2	3.42	252.25
Mn $2p_{3/2}$	Mn^{2+}	640.7	1.8	268.26
	Mn^{3+}	642.0	2.22	797.69
	Mn^{4+}	644.3	2.40	257.91
Mn $2p_{1/2}$	Mn^{2+}	652.2	1.81	112.59
	Mn^{3+}	653.6	2.16	379.26

	Mn^{4+}	655.6	2.08	88.19
Co $2p_{3/2}$	Co^{3+}	777.8	1.53	1186.84
	Co^{2+}	779.7	1.90	3231.03
	Co^{4+}	781.8	1.72	246.70
Co $2p_{1/2}$	Co^{3+}	793.0	1.49	707.34
	Co^{2+}	795.0	2.00	2254.23
	Co^{4+}	797.1	2.12	182.19
O *1s*	lattice	528.9	1.42	1142.35
	Vacancy	531.1	1.82	1387.85
	$-OH^-$	531.5	3.31	828.32

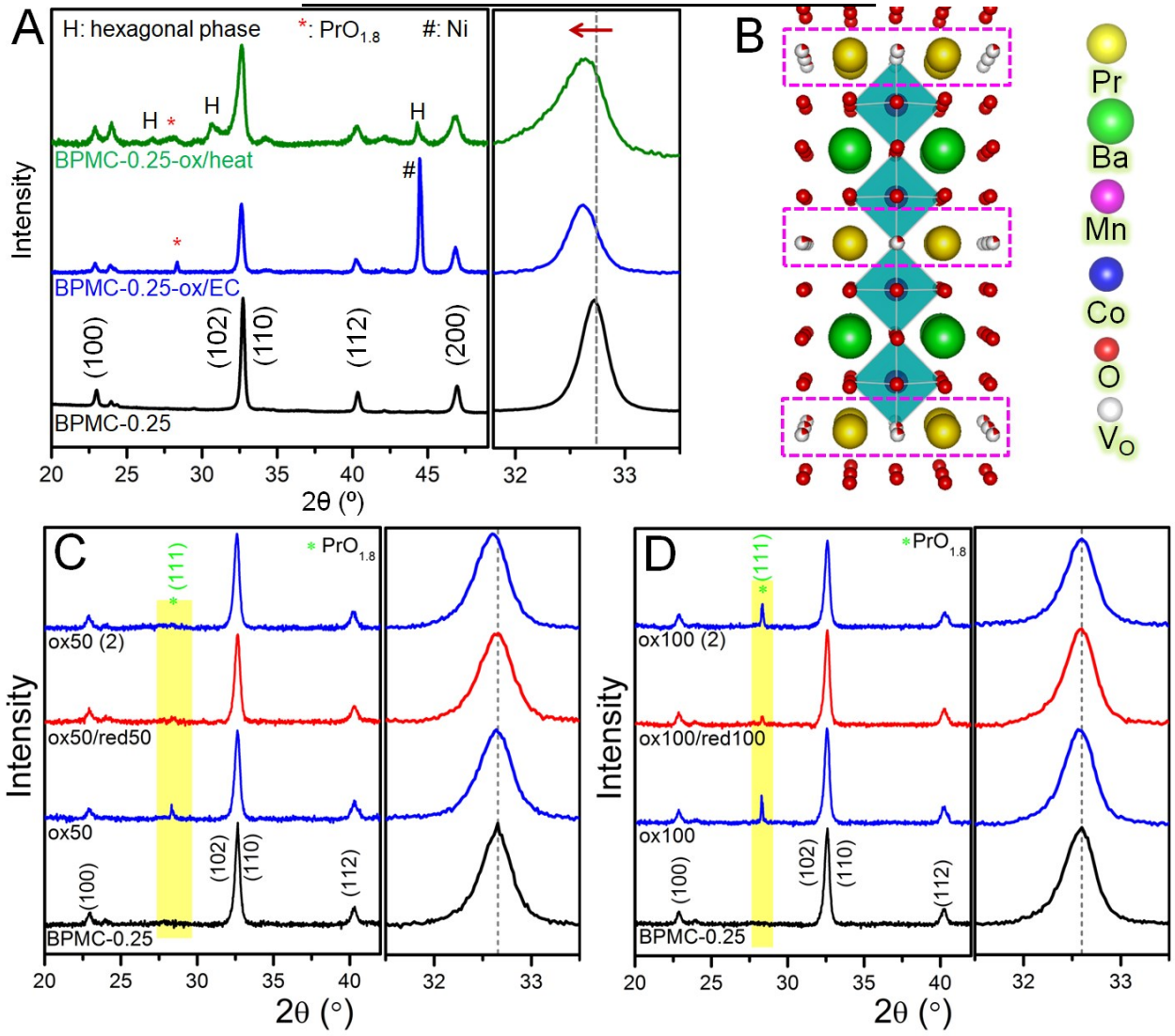

Figure S13. Electrochemical structural flexibility of BPMC-0.25. (A) PXRD patterns of BPMC-0.25, BPMC-0.25-ox/heat (oxidized under O_2 atmosphere at 500°C) and BPMC-0.25-ox/EC (oxidized by 20 CV cycles between 0 to 0.8 V). (B) Structural model showing oxygen deficient PrO_x layers of BPMC-0.25 (pink dotted box).PXRD patterns to show the effect of periodic electrochemical oxidation and reduction of BPMC-0.25 by (C) 50 cycles and (D) 100 cycles.The yellow highlighted portion highlights the (111) reflection of $PrO_{1.8}$ and the enlarged views of (110) reflection show its relative shift.

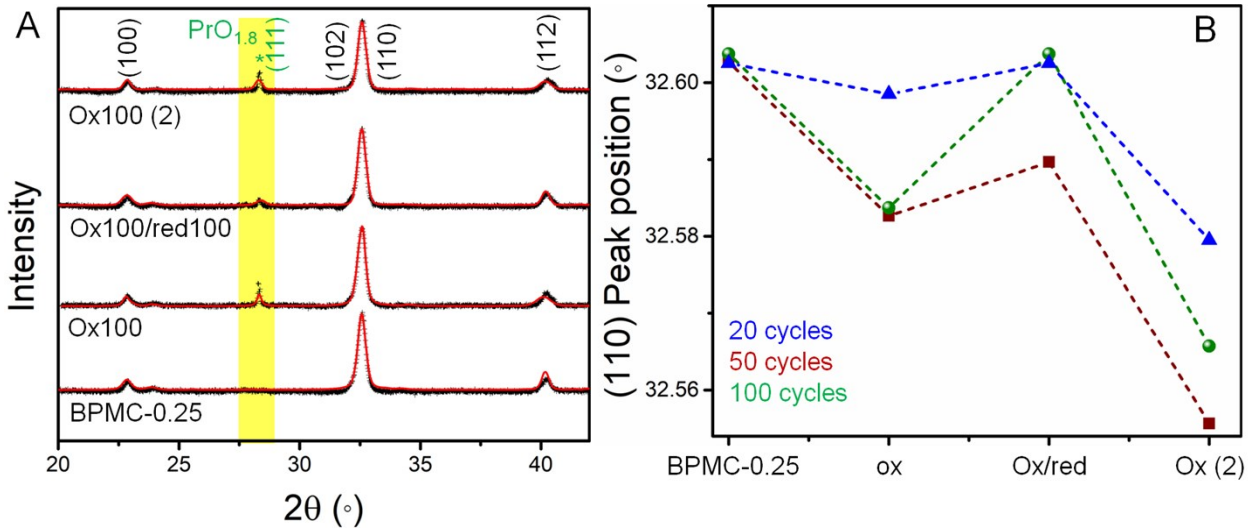

Figure S14. (A) Rietveld refinement of PXRD patterns of BPMC-0.25 samples after different electrochemical redox cycles. (B) Plots of (110) peak shift of BPMC-0.25 samples subjected to different conditions during redox experiments. A decrease in 2θ (°) corresponds to lattice expansion and vice versa.

.

Table S4. Rietveld refinement results of BPMC-0.25 NSs subjected under different electrochemical redox cycles. The space group of all the samples is *P4/mmm*.

NS samples	Phase(s)	V_{cell} (Å^3)	Lattice parameter (Å)		δ	GOF	R_w
			a	*c*			
BPMC-0.25	$BaPrMn_{1.75}Co_{0.25}O_{5+\delta}$ (impurity: 6.6 wt% $BaCO_3$)	116.9	3.8734	7.7920	0.09	2.42	2.05

BPMC-0.25-ox100	$BaPr_{0.8}Mn_{1.75}Co_{0.25}O_{5.1}$ (impurity: 2.4 wt% $BaCO_3$, 7.7 wt% $PrO_{1.8}$,)	117.2	3.8856	7.7610	0.1	2.76	2.33
BPMC-0.25-ox100/red100	$BaPr_{0.95}Mn_{1.75}Co_{0.25}O_{5.2}$ (impurity: 3.5 wt% $BaCO_3$, 2 wt% $PrO_{1.8}$)	116.8	3.8796	7.7608	0.2	2.53	2.11
BPMC-0.25-ox100/red100/ox100(2)	$BaPr_{0.8}Mn_{0.25}Co_{1.75}O_{5.2}$ (impurity: 1 wt% $BaCO_3$, 9.4 wt% $PrO_{1.8}$)	117.3	3.8917	7.7502	0.2	2.15	1.88

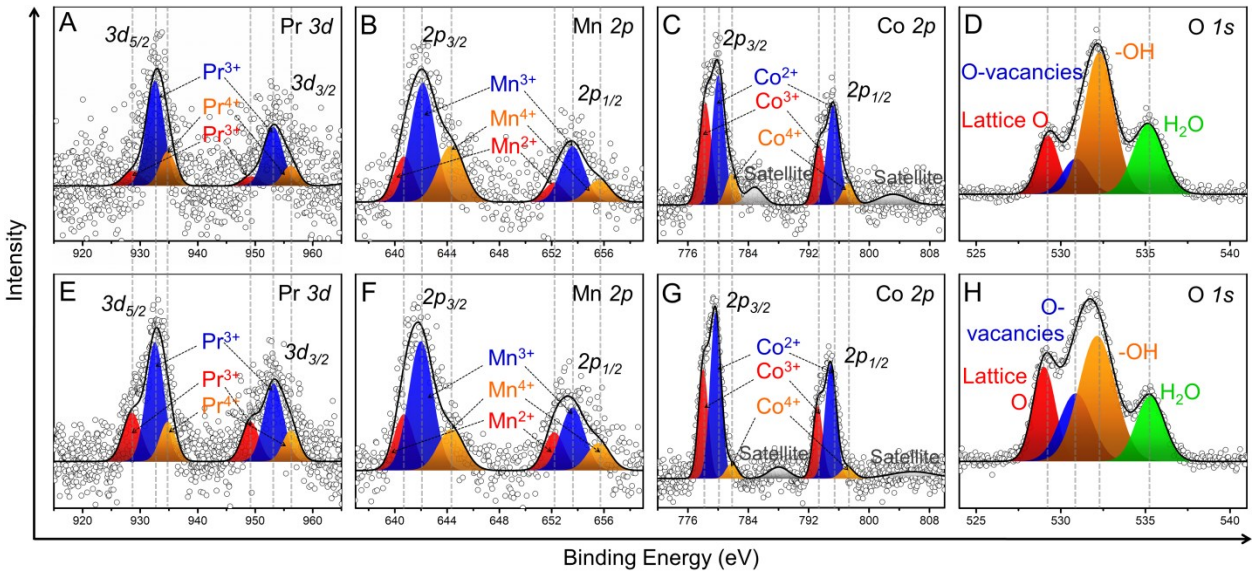

Figure S15. Fitted XPS Pr *3d*, Mn *2p*, Co *2p* and O *1s* spectra for (A-D) BPMC-0.25-ox20 and (E-H) BPMC-0.25-ox20/red20.

Table S5. XPS fitting parameters of BPMC-0.25-ox20 and BPMC-0.25-ox20/red20.

Element	State	BE	FWHM	Area	BE	FWHM	Area
		BPMC-0.25-ox20			*BPMC-0.25-ox20/red20*		
Pr $3d_{5/2}$	Pr^{3+}	928.7	3.89	45.10	928.65	3.78	261.84
		932.6	3.65	295.98	932.65	3.66	511.19
	Pr^{4+}	934.8	3.27	87.49	934.85	3.29	118.37
Pr $3d_{3/2}$	Pr^{3+}	949.3	3.57	26.24	950.15	3.54	151.03
		953.2	3.91	178.48	953.25	3.98	299.46
	Pr^{4+}	956.2	3.33	51.87	956.25	3.34	81.78
Mn $2p_{3/2}$	Mn^{2+}	640.7	1.80	44.67	640.7	1.81	71.41
	Mn^{3+}	642.1	2.22	144.48	642.0	2.20	200.41
	Mn^{4+}	644.3	2.40	73.56	644.3	2.37	68.84
Mn $2p_{1/2}$	Mn^{2+}	652.2	1.80	19.20	652.2	1.81	48.71
	Mn^{3+}	653.6	2.10	63.86	653.6	2.16	95.70
	Mn^{4+}	655.6	2.08	24.79	655.6	2.09	40.24

Co $2p_{3/2}$	Co^{3+}	778.3	1.93	290.69	778.1	1.55	309.54
	Co^{2+}	780.1	1.89	362.97	780.1	1.72	521.53
	Co^{4+}	781.8	1.81	82.73	781.8	1.75	49.46
Co $2p_{1/2}$	Co^{3+}	793.4	1.71	149.42	793.2	1.53	201.71
	Co^{2+}	795.2	1.95	287.40	794.9	1.77	368.67
	Co^{4+}	797.2	1.88	59.84	797.1	2.04	43.50
O *1s*	lattice	529.3	1.48	196.19	529.05	1.50	360.54
	Vacancy	530.9	1.86	150.43	530.65	1.60	333.68
	$-OH^-$	532.3	2.10	677.78	532.15	1.96	656.38
	H_2O	535.2	2.14	341.07	535.05	2.47	367.56

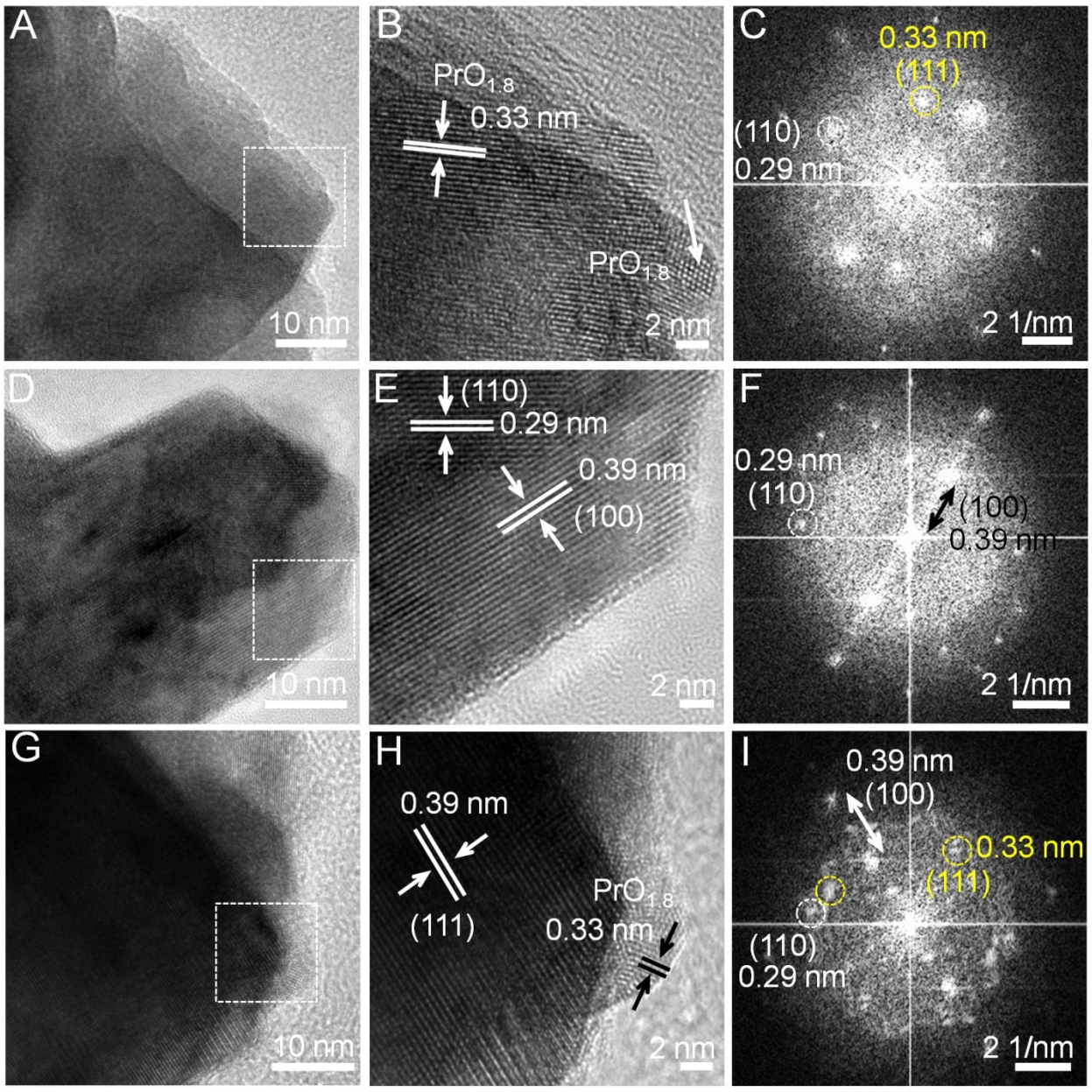

Figure S16. TEM analyses of BPMC-0.25 after electrochemical flexibility test. TEM, HRTEM images and FFT patterns after (A-C) 20 oxidation cycles (BPMC-0.25-ox20), (D-E) next 20 reduction cycles (BPMC-0.25-ox20/red20), (G-I) re-oxidation by next 20 oxidation cycles (BPMC-0.25-ox20/red20/ox (2)), respectively. The dotted squares in panels (A, D, G) represent the regions in panels (B, E, H). The white arrow in (A) indicates the $PrO_{1.8}$ phase segregation. Yellow dotted circles represent (111) reflection of $PrO_{1.8}$ while white dotted circle and arrows are the (110) and (100) plane of BPMC-0.25.

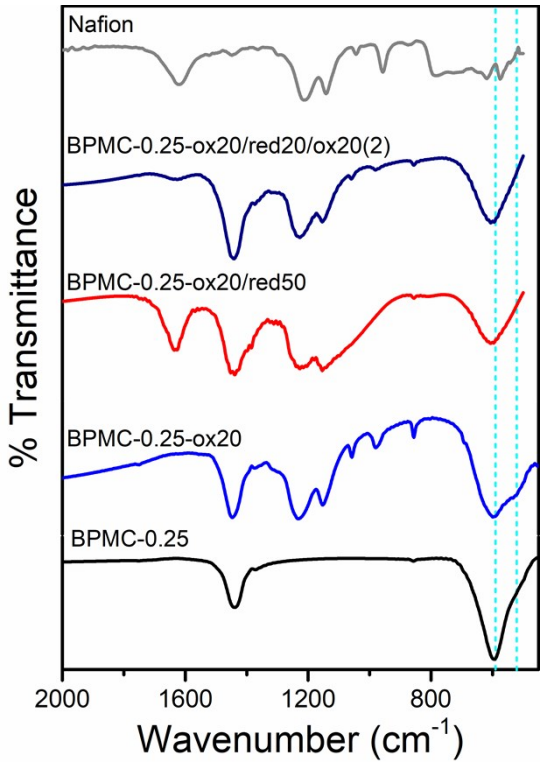

Figure S17. FTIR spectra of different BPMC-0.25, BPMC-0.25-ox20, BPMC-0.25-ox20/red20, BPMC-0.25-ox20/red20/ox (2) NSs and nafion blank.

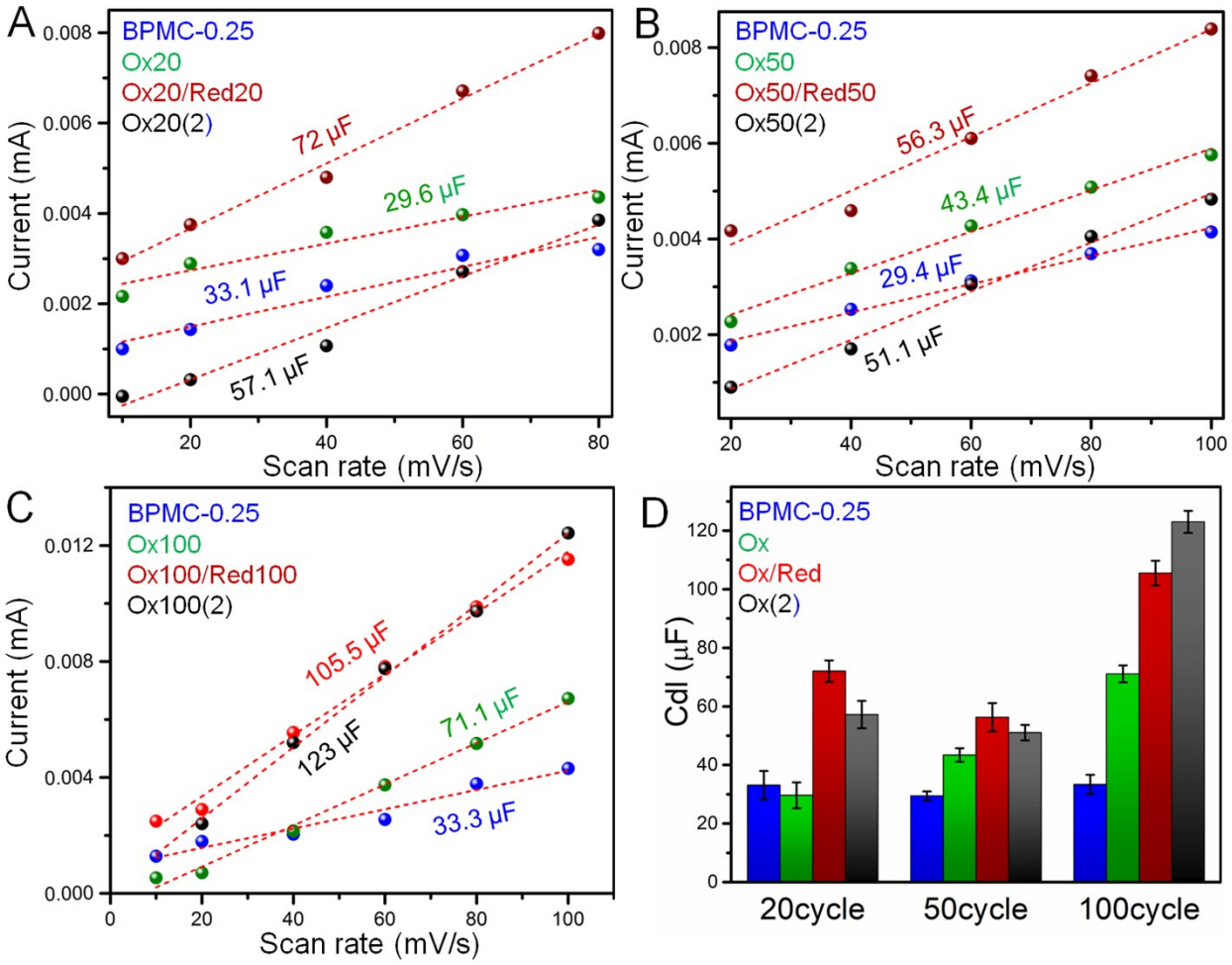

Figure S18. Double layer charge capacitance (C_{dl}) calculation of BPMC-0.25 NSs during each of the electrochemical structural flexibility tests with (A) 20 cycles, (B) 50 cycles and (C) 100 cycles of oxidation, reduction and re-oxidation. (D) Bar plots summarize the estimated C_{dl} values.

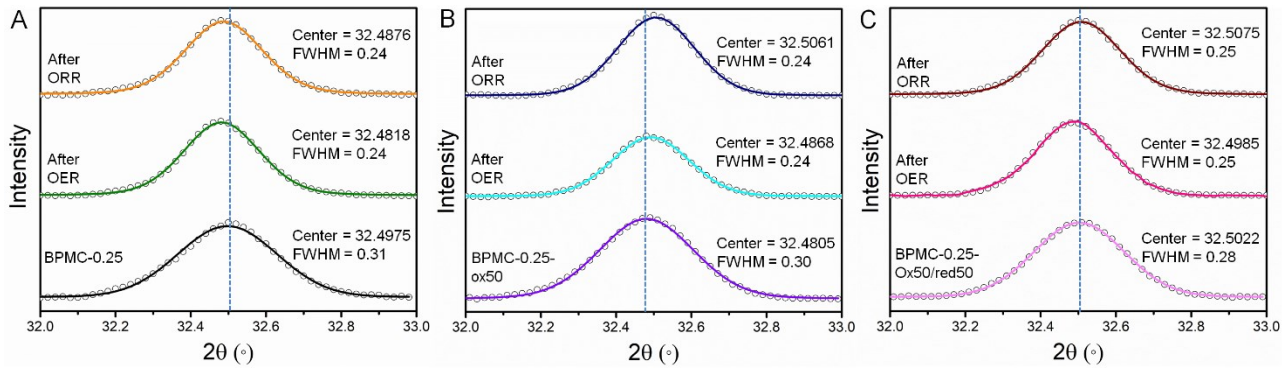

Figure S19. Fitted (110) peak of BPMC-0.25 NSs before and after *ex situ* OER/ORR: (A) pristine sample, (B) BPMC-0.25-ox50 and (C) BPMC-0.25-ox50/red50. Empty circles are experimental data while solid line is the fitted data.

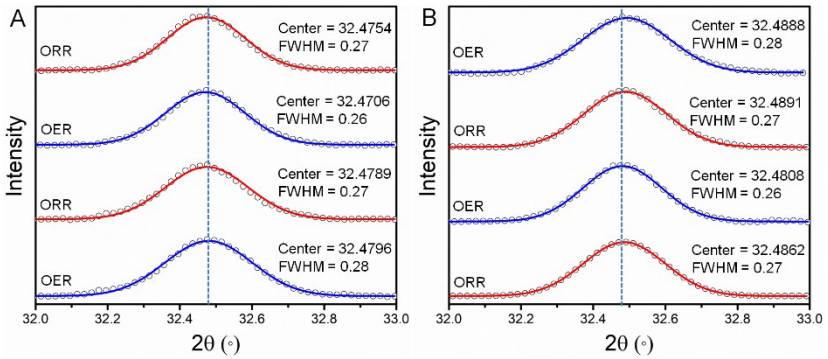

Figure S20. Fitted (110) peak of BPMC-0.25 NSs after each stage of successive (A) OER/ORR and (B) ORR/OER experiments. Empty circles are experimental data while solid line is the fitted data.

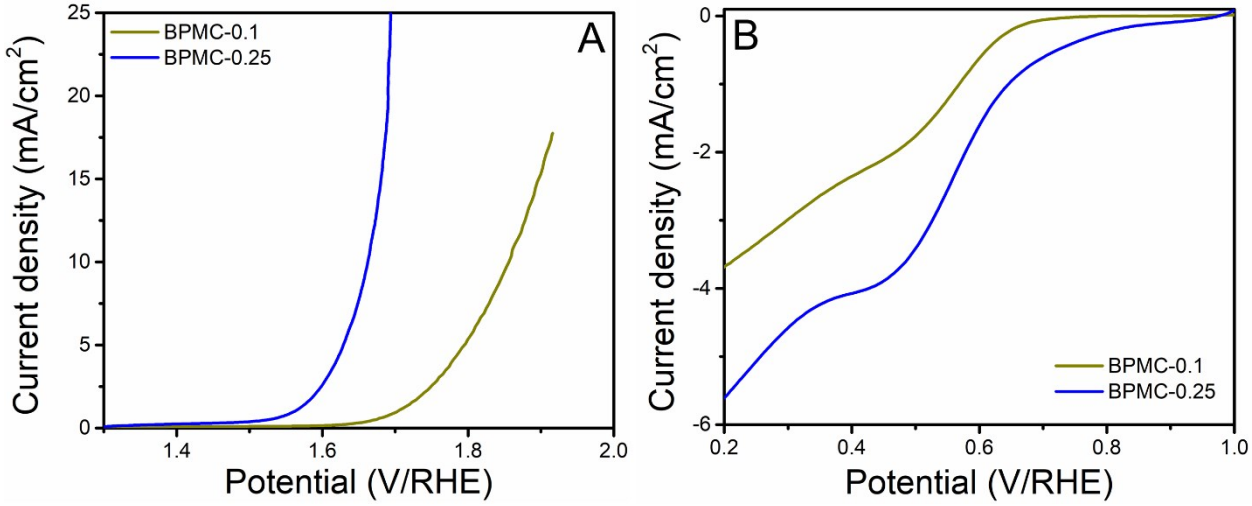

Figure S21. (A) OER and (B) ORR LSV plots of BPMC-0.1 and BPMC-0.25 NSs.

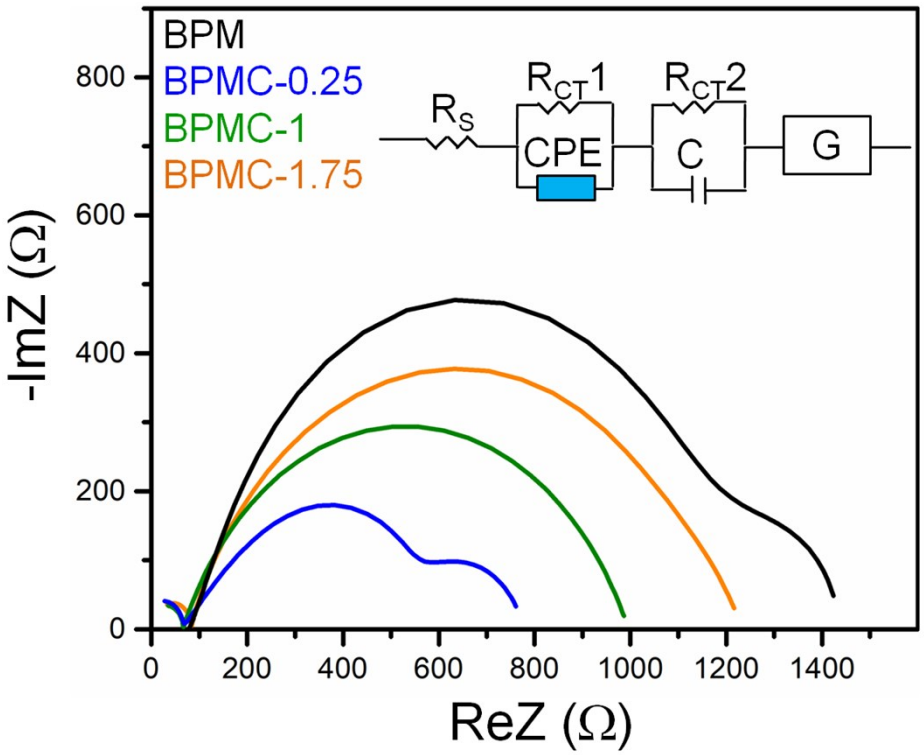

Figure S22. ORR Nyquist plots of BPMC catalysts at 0.5V bias with respect to RHE. Inset shows the corresponding equivalent circuit, where R_S, $R_{CT}1$, $R_{CT}2$, C, CPE and G are series resistance, charge transfer resistance, charge transfer resistance 2, capacitance, constant phase element and Gerischer element.[S3]

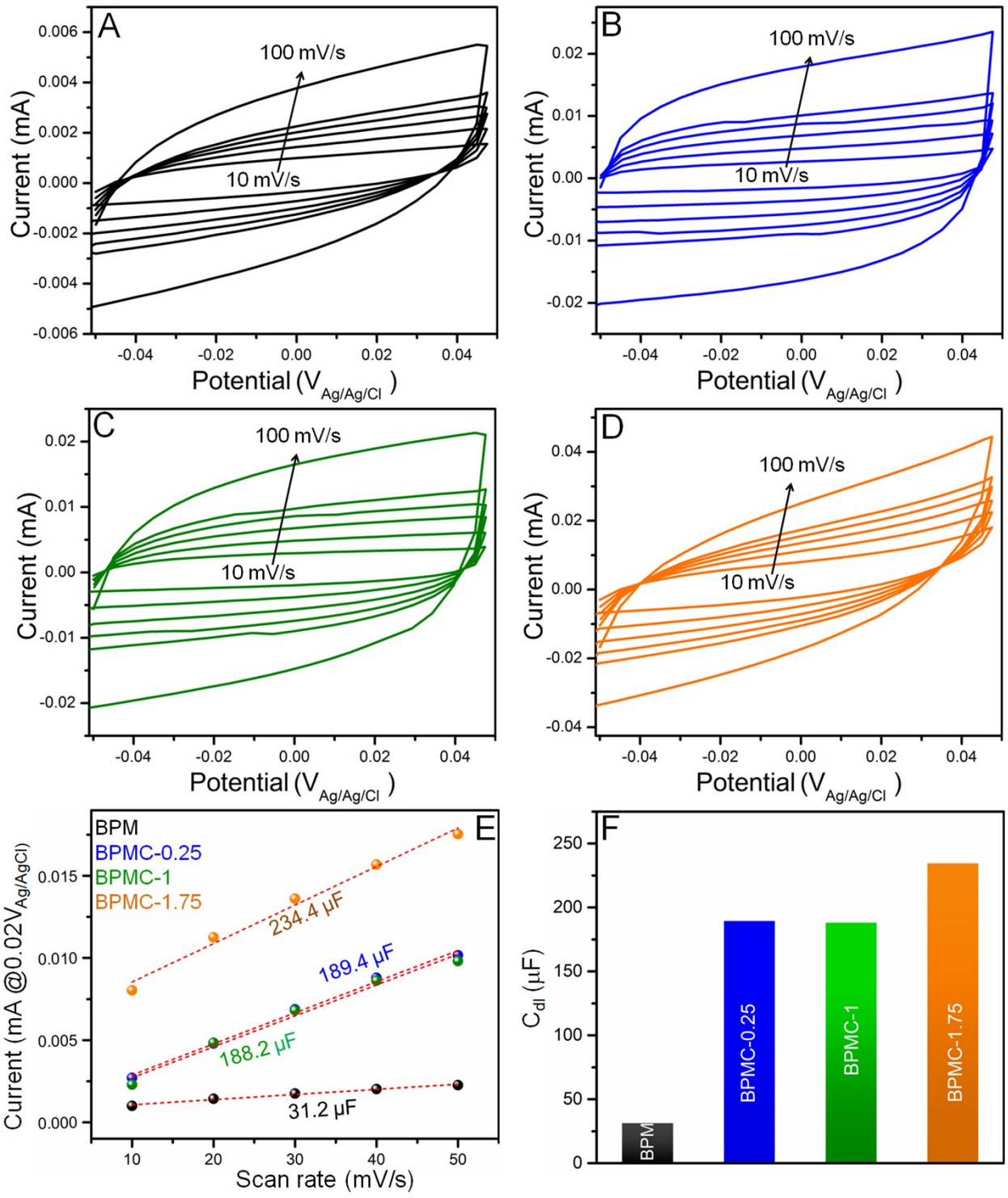

Figure S23. Determination of C_{dl} values of BPMC electrodes. CV cycles at different scan rates of (A) BPM, (B) BPMC-0.25, (C) BPMC-1and (D) BPMC-1.75. (E & F) Current-scan rate plots to determine C_{dl}.

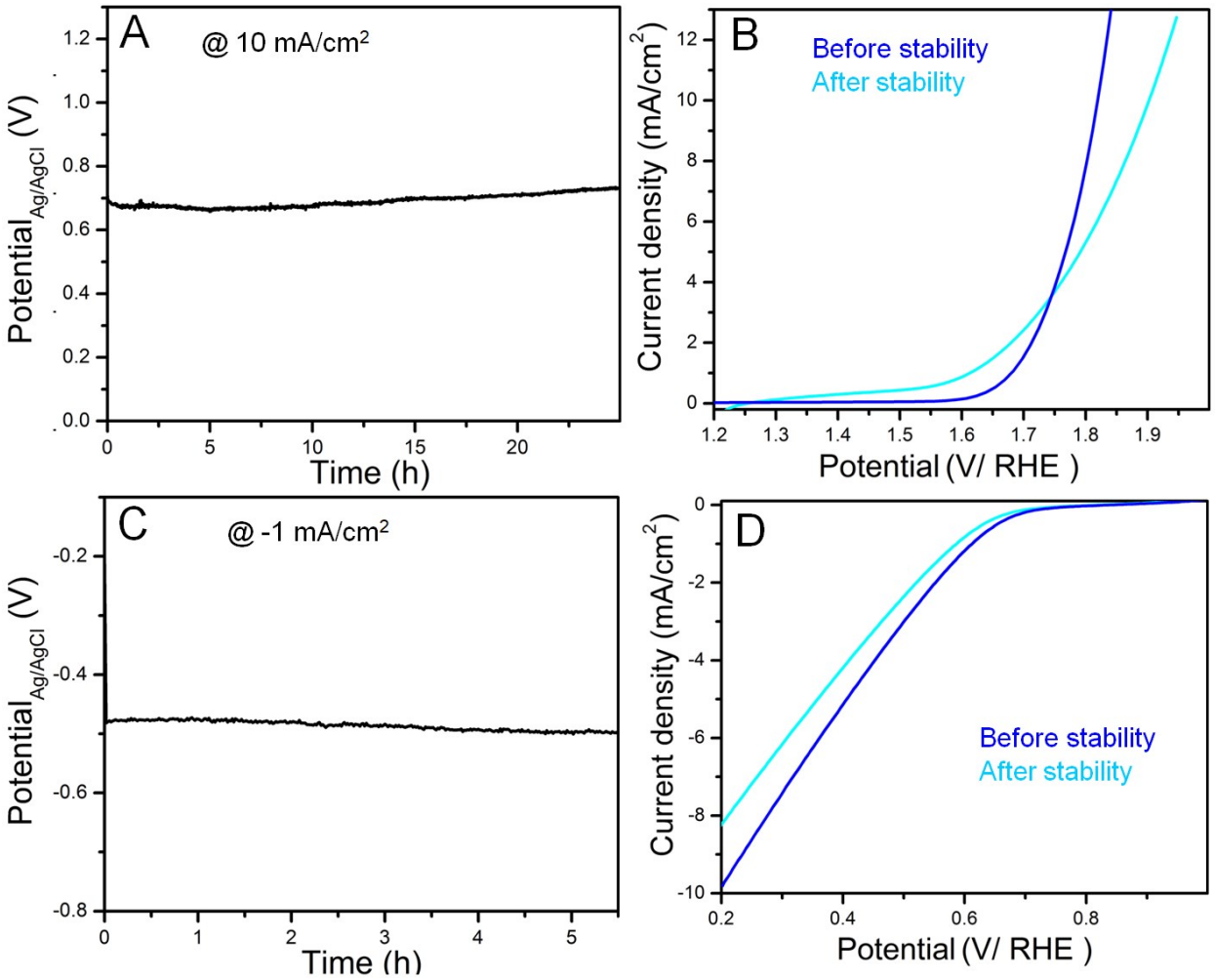

Figure S24. Chornopotentiometric (CP) stability test of BPMC-0.25 in 0.1 M KOH for (A) OER (C) ORR. Panels (B) and (D) are the corresponding LSV plots before and after CP, respectively.

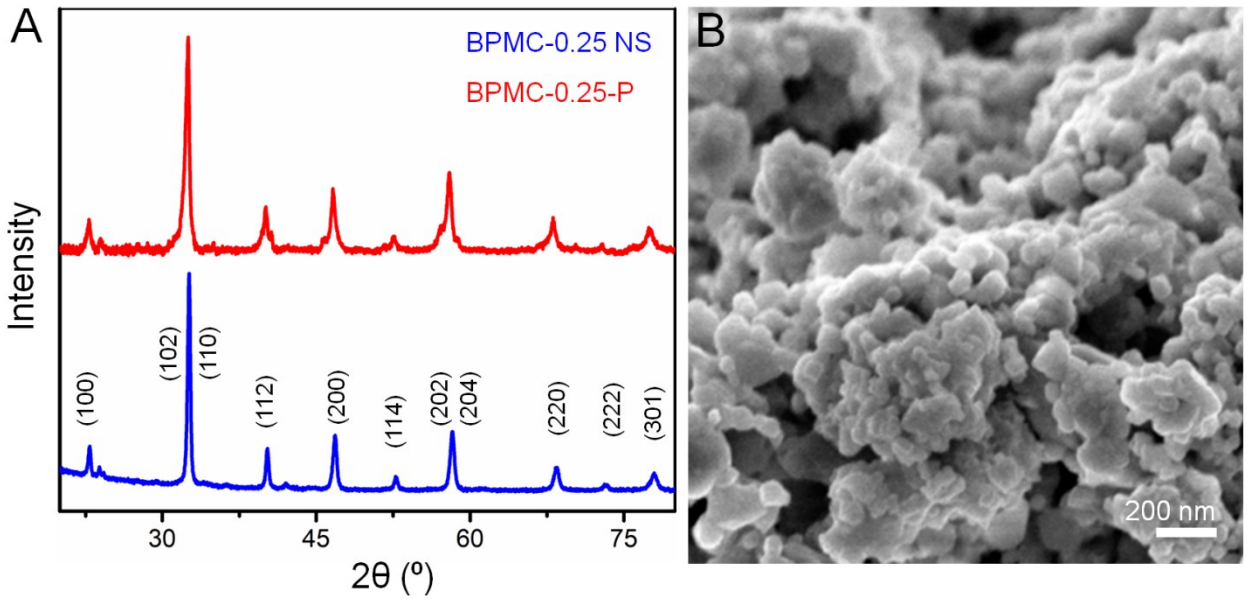

Figure S25. (A) PXRD patterns of BPMC-0.25 NS and BPMC-0.25-P (after bath sonication of BPMC-0.25 NS for 20 min in ethanol). (B) TEM image of BPMC-0.25-P.

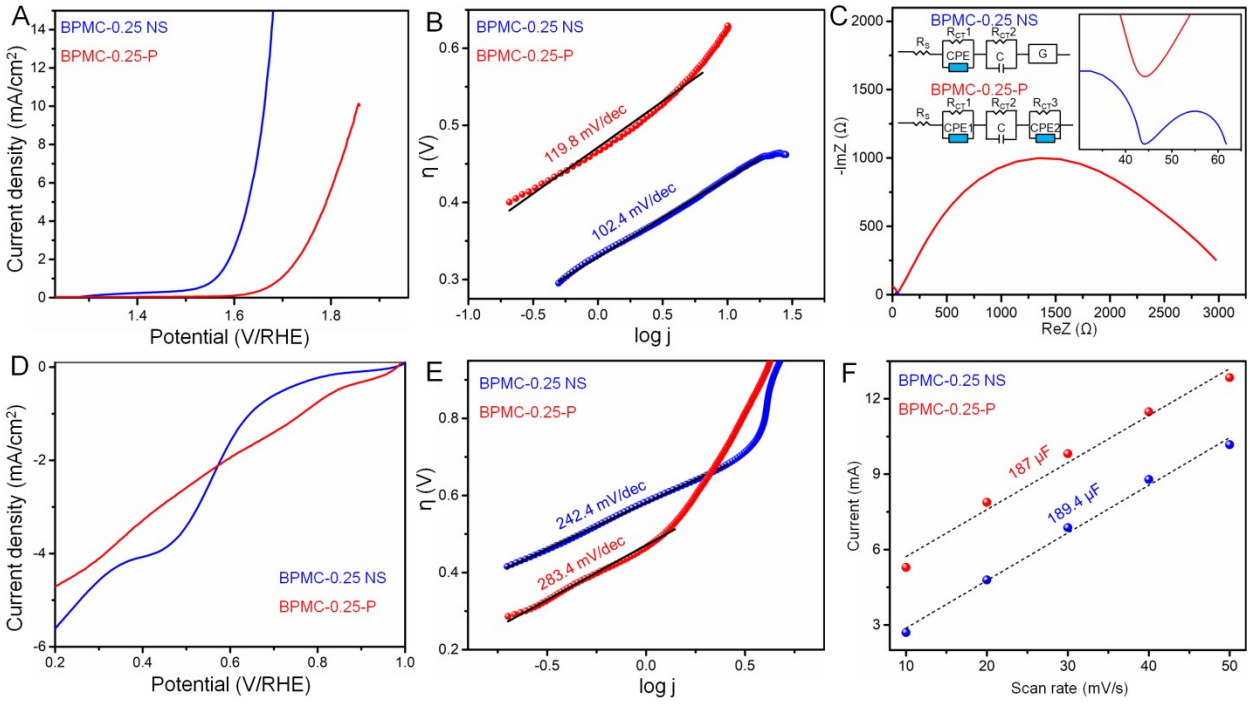

Figure S26. Oxygen electrocatalysis with BPMC-0.25 NS and BPMC-0.25-P in 0.1 M KOH. (A) OER LSV plots, (B and C) corresponding Tafel and Nyquist plots. (D) ORR LSV plots and (E) corresponding Tafel plot. (F) Plot of current at constant potential with different scan rates to determine C_{dl}.

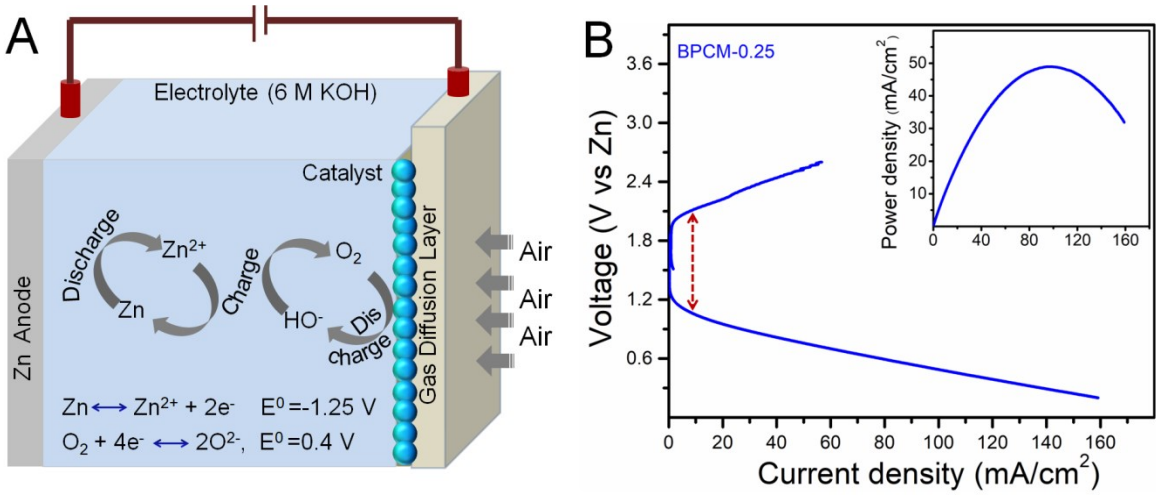

Figure S27. Activity of BPMC-0.25 cathode in homemade rechargeable Zn-air battery. (A) Schematic representation of homemade rechargeable Zn-air battery setup. (B) Polarization plots corresponding to charge and discharge. Inset shows the plot of power density as a function of current density.

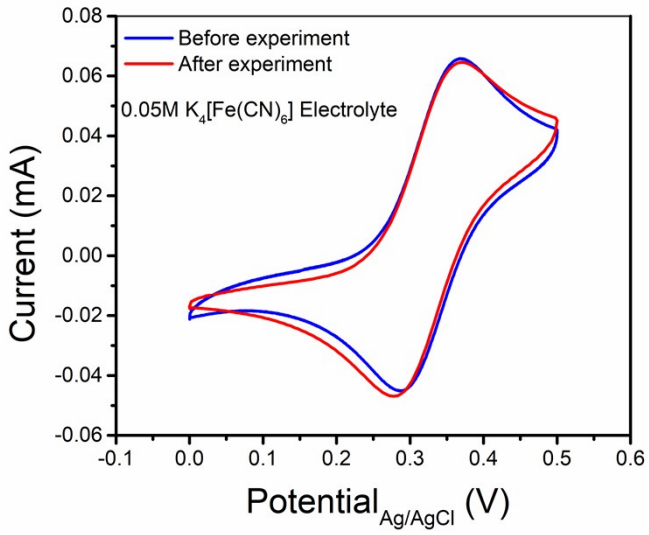

Figure S28. CV plots of 0.05M $K_4Fe(CN)_6$] demonstrating the stability of Ag/AgCl reference electrode before and after 100 CV cycles during the electrocatalytic performance of BPMC-0.25 NSs.

Table S6. Comparison of oxygen electrocatalysis activity of double perovskite oxides.

Sr. No	System	Structure	Synthesis technique	η_{ORR} (V) @ -(x) mA/cm^2	η_{OER} (V) @ 10 mA/cm^2	Ref.
1	$PrBa_{0.5}Sr_{0.5}Co_{2-x}Fe_xO_{5+\delta}$	Nanorod	Electrospin	0.85 (3)	0.3	S2
2	$PrBa_{0.85}Ca_{0.15}MnFeO_{5+\delta}$	Particle	Sol-gel	0.462 (halfwave)	0.408	S4
3	$NdBa_{0.75}Ca_{0.25}Co_2O_{5+\delta}$	Particle	Sol-gel	0.58 (3)	0.422	S5
4	$NdBa_{0.75}Ca_{0.25}Co_{1.5}Fe_{0.5}O_{5+\delta}$	Particle	Sol-gel	0.551 (3)	0.397	S5
5	$Pr_{0.5}Ba_{0.5}Mn_{1.75}Co_{0.25}O_{5+\delta}$	Nanosheet	Sol-gel	0.689 (halfwave) 0.704 (3) 0.584 (1)	0.430	This work

Supplementary References

S1 F. Dong, M. Ni, Y. Chen, D. Chen, M. O. Tadé and Z. Shao, *J. Mater. Chem. A*, 2014, **2**, 20520–20529.

S2 Y. Bu, O. Gwon, G. Nam, H. Jang, S. Kim, Q. Zhong, J. Cho and G. Kim, *ACS Nano*, 2017, **11**, 11594–11601.

S3 R. Majee, Q. A. Islam and S. Bhattacharyya, *ACS Appl. Mater. Interfaces*, 2019, **11**, 35853-35862.

S4 B. Hua, Y. F. Sun, M. Li, N. Yan, J. Chen, Y. Q. Zhang, Y. Zeng, B. Shalchi Amirkhiz and J. L. Luo, *Chem. Mater.*, 2017, **29**, 6228–6237.

S5 N. I. Kim, S. H. Cho, S. H. Park, Y. J. Lee, R. A. Afzal, J. Yoo, Y. S. Seo, Y. J. Lee and J. Y. Park, *J. Mater. Chem. A*, 2018, **6**, 17807–17818.